Korean Journal of Chemical Engineering (2024) 41:385–402
https://doi.org/10.1007/s11814-024-00122-4

REVIEW ARTICLE (INVITED ONLY)

Solid Polymer Electrolytes-Based Composite Cathodes for Advanced Solid-State Lithium Batteries

Uddhav Kulkarni[1] · Won-Jang Cho[2] · Seok-Kyu Cho[3] · Jeong-Jin Hong[2,4] · Kiran P. Shejale[2] · Gi-Ra Yi[2]

Received: 29 November 2023 / Revised: 10 January 2024 / Accepted: 13 January 2024 / Published online: 20 February 2024

Abstract

All-solid-state lithium batteries (ASSLBs) hold immense promise as next-generation energy storage systems. A crucial aspect of ASSLB development lies in achieving high energy density, which demands the high mass loadings of cathode active material. However, thick cathode with high mass loading may introduce various challenges, such as interfacial resistance between electrolytes and electrodes, suboptimal ion conduction, and limited battery lifespan. To address these challenges, composite cathode has been engineered by integrating solid-state electrolytes into conventional cathodes to enhance ion transport. Solid polymer electrolytes (SPEs), in particular, stand out for their ability to mitigate interfacial issues during cycling due to their elasticity and flexibility compared to their inorganic counterparts. This review offers a comprehensive overview of efforts to incorporate SPEs into catholytes for ASSLBs. It begins with a discussion on catholyte composition, emphasizing the properties of their constituent components. Subsequently, it provides a concise overview of electrochemical transport and measurement techniques. The review then delves into efficient and cost-effective fabrication processes, highlighting their significance. Finally, it underscores the crucial role of SPEs in advancing the development of catholytes for the future.

Keywords Solid polymer electrolyte · Catholyte · All-solid-state lithium batteries · Ion transport · Electrode design · Interfaces

Introduction

High-demand for lithium-ion batteries (LIBs) in portable electronics and electric vehicles (EVs) necessitates carbon-neutral, safe, cost-efficient, high-energy-density LIBs with lasting power [1]. Current LIBs use graphite anodes and transition metal oxide cathodes. Commercial LIBs have been developed primarily to increase their energy density and meet the demands of EV market at lower cost. However, traditional LIBs, which use highly flammable liquid electrolytes, pose significant safety risks, including lithium dendrite formation, leaks, short circuits, and fire hazards resulting from unwanted interactions between the liquid electrolytes and lithium metal or high-voltage cathode materials [2]. Therefore, there is a critical need to develop lithium-ion batteries that are safe and have high energy densities.

The replacement of liquid electrolytes with solid-state electrolytes (SEs) is a vital consideration for addressing aforementioned issues as well as eliminating the requirement for a separator. LIBs with solid electrolyte are known as all-solid-state lithium batteries (ASSLBs) which can operate with an ultra-high specific capacity and low voltage. Polymer and inorganic solid electrolytes have been intensively developed which are called solid polymer electrolytes (SPEs) and inorganic electrolytes (IEs) respectively. IEs have challenges such as high interface resistance and brittleness [3]. In contrast, SPEs offer advantages like flexibility, excellent interface compatibility, low density, enhanced safety, and ease of processing [4, 5]. However, low ion conductivity and lithium transference numbers (t_{Li+}) of SPEs are still challenging issues for their practical applications. One of

✉ Kiran P. Shejale
kiranshejale@postech.ac.kr

✉ Gi-Ra Yi
yigira@postech.ac.kr

1 Department of Chemical Engineering, Sungkyunkwan University, Suwon, Gyeonggi 16419, Republic of Korea

2 Department of Chemical Engineering, Pohang University of Science and Technology POSTECH, Pohang, Gyeongbuk 37673, Republic of Korea

3 UBATT Inc., Daejeon 34036, Republic of Korea

4 POSCO-FutureM, Sejong 30002, Republic of Korea

the key approaches is promoting local segmental motion by reducing the crystallinity and glass transition temperatures of ion channels in polymer matrices [6, 7]. These strategies accelerate lithium-ion conduction while providing the mechanical strength of SPEs. On the other hand, instability of interfacial contacts of SPE for both anodes and cathodes has been also critical issue [8]. In the case of lithium anodes, insufficient interfacial contact with the electrolyte leads to high charge transfer resistance, for which interlayer or passivation layer has been intensively investigated. Cathode experiences chemical degradation and structural changes due to uneven interfaces. The cycled use of LIBs induces the expansion and contraction of electrodes, gradually disrupting particle-to-particle interactions and diminishing overall performance [9].

To address such interfacial contact issue, SPEs are recently incorporated into cathode materials forming composite cathode (CC), which is called as catholytes. Since they provide efficient ion conduction pathways, active cathode materials can be loaded more for higher energy density of LIBs. Typically, composite cathode (CC) is composed of a mixture of active material (AM) and SPE, along with electrically conductive additives (CA) (Fig. 1a). Despite the better ionic conduction and cycle stability in catholyte, they may reduce the overall energy density of the battery. Therefore, the ratio and structure of SPE within the catholyte should be optimized for maximizing ionic conduction, energy density, and interfacial kinetics simultaneously [10].

While substantial research efforts have been directed towards enhancing the conductivity of solid polymer electrolytes (SPE) and their compatibility with lithium anodes, there has been a limited focus on improving the stability and compatibility of interfaces, between SPE and cathode assemblies. Interfacial kinetics within catholyte can be improved by inhibiting strong surface oxidation of cathode material at high voltages through catholyte surface modification with SPE considering their compatibility and oxidation reactivity [11]. Further, to mitigate the chemical degradation of the catholyte interface, various types of interlayer coatings in catholyte have been employed [12–15]. Also, concurrent high ionic conduction, energy density, and stable interfacial kinetics in ASSLBs may be possible by inclusion of ionic conductor additives in SPE matrix which can create fast-ionic transport pathways and stable SPE/CA interface.

Understanding the complex, evolving interfacial dynamics within the catholyte is crucial in achieving high-capacity and high-performance ASSLBs, which requires meticulous design of the catholyte's components and architecture, along with thoughtful construction methods to ensure efficient conduction of Li^+ and electrons, as well as interface stability. In this article, we will briefly explore the impact of critical parameters of the catholyte on the energy density of ASSLBs. The first section focuses on electrode design for catholytes, emphasizing the role of SPE within the catholyte, understanding of interfacial dynamics, transport properties and stability using AM, SPE, and CA. Discussion also include the significance of catholyte's design parameters, such as catholyte composition, structure, voids and preparation approach for high ionic transport and energy density. Table 1 summarizes the recent advancements in SPE-based catholytes. The electrochemical transport and measurement techniques in catholyte covers ion transport, ionic (σ_i) and electronic (σ_e) conductivity and lithium-ion transference number (t_{Li+}). Since the cathode significantly influences the

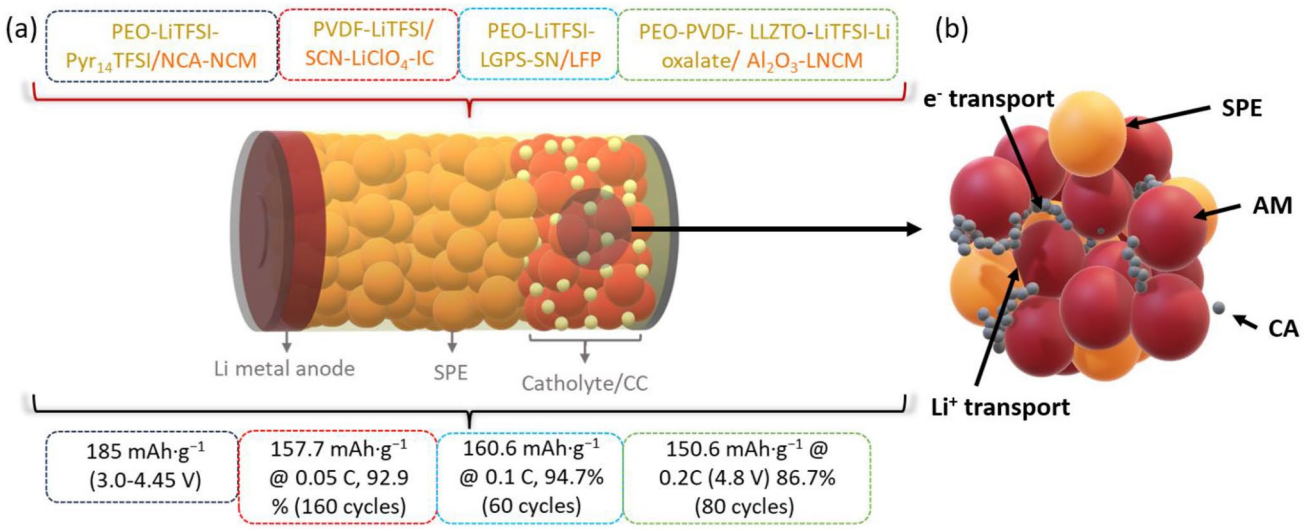

Fig. 1 **a** Schematic illustration of the catholyte ASSLBs along with several experimental data in previous reports [8, 10, 16, 17] and **b** catholyte components and electrochemical transport in ASSLBs, solid polymer electrolytes (SPEs), active material (AM) and conductive additives (CA)

Table 1 Cell configuration, characteristics, and electrochemical performance of catholytes in advanced ASSLBs

Cell configuration	Catholyte				Preparation	Loading level/σ/τ_+/V vs. Li/Li^+ (mg cm^{-2}/S cm^{-1} –/–)	Cycling performance (capacity/C-rate/°C/capacity retention	Energy density (Wh/kg)[a]	References
	Li salt	Solvent	SPE	Cathode composition (CC)					
Li/LiBC/CC-LFP	LiMTFSI	Water	PEGM/LiMTFSI (LiBC)	CC = LFP/LiBC-1/CB (60/30/10)	Reversible addition-fragmentation chain transfer polymerization technique	–/1.2×10^{-5}/0.83 @ 55 °C/4.5	130 mAh g^{-1}/(C/15)/–/–	442	[18]
Li/PEO_{15}LiFSI/CC-NMC	β-Li_3PS_4	Oppanol/toluene	PEO/LiTFSI (1/15)	CC = β-Li_3PS_4/NMC 622/Super C65 or vapor grown carbon fibers/Oppanol (28.8/67.2/2/2)	Solvent-free, hot-pressing process double-coating/cold-pressing	8.6/–/–/–	140 $mAhg^{-1}$/(C/20)/60 °C/90%-(50 cycles)	510	[19]
Li/50[PEO_8-LiTFSI]-40LLZTO-10PVDF + 9% OX/CC-Al_2O_3@NCM	LiOH/LiTFSI	DMF	PEO/PVDF/LLZTO/LiTFSI/oxalate (8/10/40/1/9)	CC = Al_2O_3@NCM/superP/PVDF (95/2/3)	Solvent-casting	2,5,10/2.0×10^{-4}/0.45 @ 55 °C/4.8	150.6 mAh g^{-1}/0.2 C/55 °C/86.7%-(80 cycles)	572.3	[10]
Li/LiRCC1-ClO_4/CC- LFP	$LiClO_4$	Ethanol/water (v:v = 3:1)/NMP	Li/cationic amine cage framework (RCC1)/ClO_4	CC = LFP/AB/CNTs/PVDF/Li-RCC1-ClO_4 (71/4/2/3/20)	Solvent evaporation and grows	1/5.13×10^{-5}/0.7 @ 55 °C/5	135 mAh g^{-1}/0.5 C/RT/100% (200 cycles)	472.5	[20]
Li/$P(EO)_{10}$LiTFSI-($Pyr_{14}TFSI)_2$/CC-	LiTFSI	–	PEO/LiTFSI/$Pyr_{14}TFSI$ (10/1/2)	CC = LFP/NCM, NCA/C/PEO/LiTFSI/$Pyr_{14}TFSI$ (43/43/7/17.5/5/27.5)	Solvent-free, hot-pressing process	3–4 (LFP), 4–5 (NCM, NCA)/–/–/4.45(NCA)	161 (LFP), 157 (NCM), 185 (NCA) mAh g^{-1}/(C/20)/40 °C/60%(NCA)-(100 cycles)	–	[16]

Table 1 (continued)

Cell configuration	Catholyte				Preparation	Loading level/σ/τ_+/V vs. Li/Li^+ (mg cm^{-2}/S cm^{-1} –/–)	Cycling performance (capacity/C-rate/°C/capacity retention	Energy density (Wh/kg)[a]	References
	Li salt	Solvent	SPE	Cathode composition (CC)					
Li/PEO-LiTFSI—LGPS-SN/CC-LFP	$LiClO_4$	Anhydrous ACN	PEO/LiTFSI-/LGPS/SN (1/10)	CC = LFP/Super-P/PEO-$LiClO_4$ (7/2/1)	Conventional solution-casting technique	–/9.10×10^{-5}/0.2 @ 25 °C/5.5	160.6 mAh g^{-1}/0.1 C/40 °C/94.7%-(60 cycles)	543	[8]
Li/CC-PEDOT-LFP	LFP	–	–	CC = PEDOT- LFP	Dynamic three phase interline electropolymerization	10.8–13.2/–/–/4	75 mAh g^{-1}/(C/10)/–/69%	255	[21]
Li/PS-b-PEO-b-PS/CC- LFP	LiTFSI	Dichloromethane/I [50:50 (v/v)]	PS-b-PEO-b-PS	CC = LFP/PS-b-PEO-b-PS/C (60/32/8)	Solvent-casting	–/5×10^{-4}@ 80 °C/0.15/3.8	130 mAh g^{-1}/(C/8)/60 °C/fully recovered	442	[22]
Li/PLLS15/CC-LFP	LiTFSI	ACN	Al-LLZO and SN	CC = LFP/Al-LLZO/SN (80/10/10)	Solvent-casting	1–2/4.17×10^{-4}/0.451/4.65	130 mAh g^{-1}/(20 mA g^{-1})/25 °C/89% (200 cycles)	442	[23]
Li/PEO-LiTFSI/CC-LFP	LiTFSI	I/NMP	SI-PPO-PEO-LiTFSI	CC = LFP/SI-PPO-PEO LiTFSI/C65 (63/30/7)	Solvent-casting	2.8–4.9/5.3×10^{-4} S cm^{-1} @ 70 °C/ 0.38/4	168 mAh g^{-1}/(C/10) 70 °C/92% (100 cycles)	588	[24]
Li/PVCA-LiDFOB/CC-LCO	LiDFOB	–	PVCA-LiD-FOB	CC = LCO/PVCA/Acetylene black (80/10/10)	Solvent-casting	1.5/9.82×10^{-5} S cm^{-1} @ 50 °C/0.57/4.5	146 mAh g^{-1} (C/10)/50 °C/84% (150 cycles)	613.2	[25]
Li/PVDF-LiFSI/CC-LCO	LiFSI	–	PVDF-LiFSI	CC = LCO/PEO/SuperP/LiTFSI (75/11/10/4)	–	2.8/1.18×10^{-4} S cm^{-1} @ 25 °C/–/3.96	141 mAh g^{-1}/(0.15 mA cm^{-2})/25 °C/100% (200 cycles)	–	[26]
Li/PI-LLZTO-PVDF/CC-NMC 532	LiTFSI	NMP	PI-PVDF/LLZTO	CC = NCM 532/PVDF/Super P/SN/LiTFSI (81.1/4/6.75/1.4)	Solvent-casting	9–10/1.85×10^{-4} S cm^{-1} @ 25 °C/0.51/4.8	152.6 mAh g^{-1}/(C/10)/25 °C/94.9% (80 cycles)	600	[27]
Li/P(STFSILi)-PEO/CC-LFP	LiTFSI	Water	P(STFSILi)-PEO	CC = LFP/P(STFSILi)-PEO/carbon black (60/32/8)	Solvent-casting	–/1.3×10^{-5} S cm^{-1} @ 60 °C/0.85/5	138 mAh g^{-1}/2 C/60 °C/(80 cycles)	483	[28]
Li/LAGP-PEO-LiTFSI/CC-LFP	$LiClO_4$	ACN	PEO- $LiClO_4$	CC = LFP/super P/PEO- $LiClO_4$ (55/10/35)	Solvent-casting	3.6 mg cm^{-2}/1.9×10^{-4} S cm^{-1} @RT/–/4.75	137.6 mAh g^{-1} (0.2 C)/55 °C/91.3% (100 cycles)	481.6	[29]

Table 1 (continued)

Cell configuration	Catholyte				Preparation	Loading level/σ/τ_+/V vs. Li/Li^+ (mg cm^{-2}/S cm^{-1} –/–)	Cycling performance (capacity/C-rate/°C/capacity retention	Energy density (Wh/kg)[a]	References
	Li salt	Solvent	SPE	Cathode composition (CC)					
Li/PEO-LiTFSI + LLZO nanowires/CC-LFP	LiTFSI	–	LLZO nanowires -PEO-LiTFSI	CC = LFP/PEO-LiTFSI/carbon black (80/10/10)	–	1.68 mg cm^{-2}/ 2.39×10^{-4} S cm^{-1} @ RT/–/5.5	162.9 mAh g^{-1}/(0.1 C)/60 °C/97.4% (80 cycles)	570.2	[30]
Li/LPSCl-SPE/CC-$LiNbO_3$ @ NMC811	LiTFSI	Anhydrous THF	LPSCl/PC-PEO-PC/LiTFSI	CC = NMC811/LPSCl/PC-PEO-PC/CNF 70/23/5/2	Solvent casting	15/9.1 × 10^{-3} S cm^{-1} @ 60 °C/0.62/4	–/0.5 C/60 °C/86% (200 cycles)	–	[31]
Li/LLZO/PEO + $LiClO_4$/CC-NCM	$LiClO_4$	ACN	LLZO/PEO-$LiClO_4$	CC = NCM622/PEO/LLZO/$LiClO_4$/SPB (56/15/21.5/2.5/5)	Slurry casting	2.0/4.42 × 10^{-4} S cm^{-1} @ 55 °C)/–/5	189 mAh g^{-1}/0.02 C/55 °C/87.8%	700	[32]
Li/LAGP/PEO-$LiClO_4$/CC-LFP	$LiClO_4$	ACN	LAGP/PEO-$LiClO_4$	CC = LFP/PEO/$LiClO_4$/SN/SuperP (50/30.86/4.14/5/10)	Slurry casting	8/1.1 × 10^{-4} S cm^{-1}/–/5	136.8 mAh g^{-1}/0.2 C/25 °C/(20 cycles)	478.8	[33]
Li/PPC/LiTFSI/LLZTO /CC-LFP	LiTFSI	–	PPC/LiTFSI/LLZTO	CC = LFP/PPCL-SPE/carbon black (80/10/10)	–	–/5.2 × 10^{-4} S cm^{-1} @ 20 °C/0.75/4.6	110 mAh g^{-1}/1 C/20 °C/95% (800 cycles)	352	[34]
Li/PEO-LAGP/CC-LFP	LiTFSI	–	PEO-LAGP	CC = LFP/PEO-LAGP/SuperP (70/20/10)	–	–/6.76 × 10^{-4} S cm^{-1} @ 60 °C/0.37/5.3	166 mAh g^{-1}/0.1 C/60 °C/close to 90% (50 cycles)	564.4	[35]
Li/PEO- LiTFSI-LLZ/CC-NCM622	LiTFSI	ACN	PEO- LiTFSI-LLZ	CC = NMC622/PEO-LiTFSI-LLZ/C65 (75/20/5)	Slurry casting	–/3.0 × 10^{-4} S cm^{-1} @ 25 °C/4.2	150 mAh g^{-1}/(C/20)/–/–	555	[36]
Li/PEO-LLTO – SN/CC-NCM532	LiTFSI	ACN	PEO-LLTO–SN	CC = NCM532/PEO-LiTFSI-SN/C65/PVDF (70/15/10/5)	Slurry casting	–/2.4 × 10^{-3} S cm^{-1} @ 55 °C/–/5	143.2 mAh g^{-1}/(C/20)/55 °C/-(30 cycles)	529.8	[37]
Li/PVDF-LLZTO-$LiClO_4$/CC-LCO	$LiClO_4$	NMP	PVDF-LLZTO-$LiClO_4$	CC = LCO/PVDF-LLZTO-$LiClO_4$/SuperP (8/1/1)	Slurry casting	1.9/5 × 10^{-4} S cm^{-1} @ 25 °C/–/4.2	150 mAh g^{-1}/0.4 C/25 °C/98% (120 cycles)	585	[38]
Li/PEO-Al-LLZTO- LiTFSI/CC-LFP	LiTFSI	ACN	PEO-Al-LLZTO-LiTFSI	CC = LFP/PEO-LiTFSI/ITO	Slurry casting	–/2.48 × 10^{-4} S cm^{-1} @ 30 °C (60wt% Al-LLZTO)/–/–	155 mAh g^{-1}/–/60 °C/97% (10 cycles)	496	[39]
Li/CSPE/CC-LFP	LiTFSI	NMP	PPC-LiTFSI-SiO_2	CC = LFP/PPC-LiTFSI/SuperP (70/20/10)	Slurry casting	/8.5 × 10^{-4} S cm^{-1} @ 60 °C/0.86/4.8	156 mAhg^{-1}/0.1 C/60 °C/86% (100 cycles)	514.8	[40]

[a]Energy density (Wh kg^{-1}) values are estimated using gravimetric capacities and working voltages [41]

capacity of ASSLBs, it is important to pay close attention to catholyte processing and preparation. We discussed various efficient and cost-effective fabrication techniques for catholytes. Finally, we outline the key hurdles and difficulties in enhancing catholyte for ASSLBs and present suggested approaches to overcome these challenges.

Design of Catholytes

In advanced all-solid-state lithium batteries (ASSLBs), catholytes play a crucial role in optimizing both gravimetric and volumetric energy densities while ensuring effective conductivity for both Li^+ ions and electrons. In catholyte, the SPE serves as a binder as well as an electrolyte which provides mechanical stability and form solid interfaces with continuous pathways for efficient electronic and ionic conduction (Fig. 1b). The energy density of catholytes is influenced by component ratios, structural design, interfaces and test conditions. Due to the diverse range of influencing factors, it remains challenging to propose a precise and universally applicable calculation model for highly efficient ASSLBs. Table 1 provides a summary of reported cell chemistry, SPE type, catholyte composition, fabrication details, and their corresponding electrochemical performance.

Solid Polymer Electrolytes (SPEs)

Being one of the main ingredients of catholyte, solid polymer electrolytes (SPEs) are typically composed of polymer matrices and lithium salts with low mass densities and lack the liquid solvents. They are chemically stable, cost-effective as well as compatible with large-scale manufacturing processes and show mechanical resilience at temperatures above the glass transition point (T_g) [42]. The polymer matrices for solid polymer electrolytes (SPEs) need to exhibit distinct properties. These include a well-balanced interaction with cations to ensure solubility and ionic mobility, a high dielectric constant for effective charge separation, optimal backbone flexibility to minimize energy barriers for ionic transport, and a substantial molecular weight to bolster mechanical strength [43].

The minimal ion-pair dissociation in an electrolyte is one of the limiting factors for cationic transport in hydrocarbon polymer based SPE such as ε polyethylene and polypropylene with a low dielectric constant ($\varepsilon < 5$). In contrast, polymers with electron-withdrawing groups, carbon-carbon backbones, and ion-pair dissociation with specific non-classical effects, have garnered significant attention in the field of SPE-catholyte research, which include poly(ethylene oxide) (PEO), poly acrylonitrile (PAN), poly methyl methacrylate (PMMA), and poly vinyl alcohol (PVA). Specifically, polyethylene oxide (PEO) has been extensively studied in the context of SPEs-catholyte owing to its notable capacity to dissolve lithium salts [51]. However, gradual oxidation of PEO-based SPEs at potentials exceeding 3.9 V falls short of the requirements for high-voltage cathodes [52]. Resembling coordination of Li ions with the ether oxygen of PEO, polycarbonate and polyester can also form coordination bonds with Li ions through their carbonyl and ether oxygen atoms, exhibiting similar characteristics to some extent. Poly ethylene carbonate (PEC), poly trimethylene carbonate (PTMC), poly vinylene carbonate (PVCA), and poly propylene carbonate (PPC) offer favorable polycarbonate matrices for SPEs, demonstrating impressive ionic conductivities of up to 10^{-4} S cm^{-1} and an electrochemical window surpassing 4.5 V [53, 54]. In contrast, alternative polymer types such as polyvinylidene fluoride (PVDF), PVDF-hexafluoropropylene (PVDF-HFP), polycarbonates, and PAN have been reported to remain stable at voltages over 4.5 V (Fig. 2b) [25, 44–50]. However, it is crucial to consider that the actual decomposition potentials for SPEs are likely to be lower than the measured values, given the sluggish reaction kinetics observed under various test conditions. Moreover, the extended interfacial contact between the polymer and cathode materials within composite cathodes can further accelerate the oxidation of SPEs [55, 56]. Figure 2a demonstrates the various chemical structures of typical polymers in SPEs in catholyte.

Also, SPEs in catholyte can be designed to inhibit crystallization through the addition of plasticizers, polymer blending, or the incorporation of nanoparticles tethered to oligomers. Also, incorporating ionic liquids into the backbone, crosslinking sites, or as side groups proves to be effective in achieving high ionic conductivity across a broad temperature range, particularly beneficial for electric vehicles [57–59]. Approaches to boost the ionic conductivity of SPEs-catholyte include augmenting the free volume within the electrolyte, which can be achieved by introducing plasticizers or through the retention of residual solvents [49]. Interestingly, higher levels of Li salt can be incorporated into the polymer matrix, in which lithium salts serve as effective plasticizers. Polysiloxanes with low T_g exhibit high ionic conductivity due to the flexibility of the Si–O–Si bond. Furthermore, bifunctional PEO polymers are added into polysiloxanes as crosslinker, which creates interpenetrating networks resulting in a high ionic conductivity of 1.62×10^{-4} S cm^{-1} [60].

Apart from the above mentioned SPEs, polymeric ionic liquids (PILs) are a special class of SPEs, where polymer backbones consist of ionic side chains. Self-healable PILs have garnered significant interest due to their uniformly dispersed charging units throughout the structure, and the preference for PILs with charged scaffolds is driven by their compatibility and affinity with the polymer matrix, allowing for enhanced self-healing capabilities through enriched ion-ion interactions [61, 62]. For example, imidazolium IL

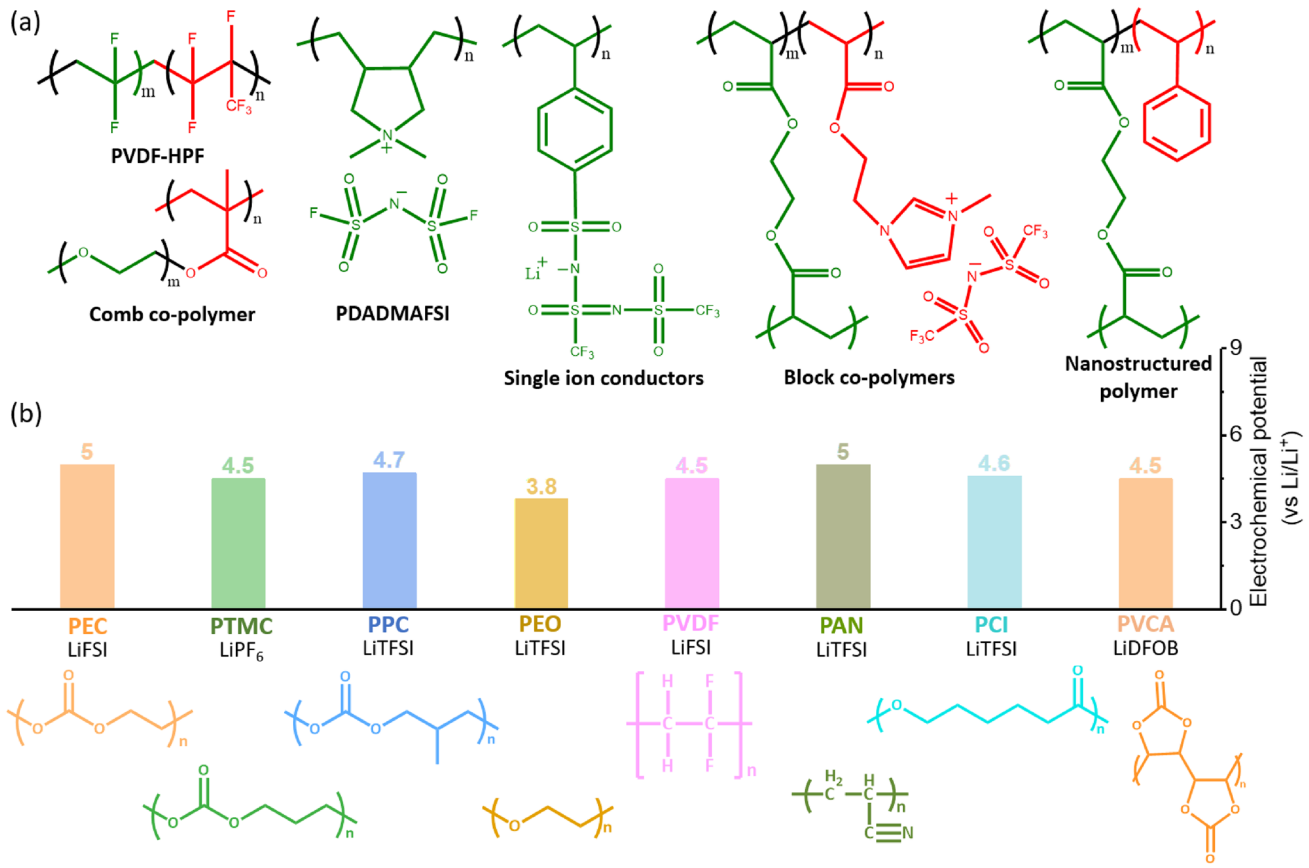

Fig. 2 **a** Chemical structures of typical polymers in SPEs and **b** electrochemical potential vs. Li/Li^+ of SPEs for high-voltage operation [25, 44–50].

and ethyl acrylate were employed in the development of self-healable PIL through statistical copolymerization, followed by counter-anion exchange from Br^- to bulkier ions such as Otf^-, FSI^-, and $TFSI^-$. Notably, the PIL-SPE containing $TFSI^-$ counter-ions exhibited complete healing of damage when heated at 55 °C for 7.5 h, achieving an ionic conductivity of 1.6×10^{-7} S cm^{-1} at 25 °C [63]. In PIL-based SPEs, crystalline behavior of the polymer and ion-polymer interactions determines the ion transport efficiency [64]. Recent advancements have introduced SPEs utilizing PDADMAFSI based PILs and a high concentration of LiFSI salt, where FSI anions are coordinated by cationic polymer backbone and Li ions. Molecular dynamics simulation revealed that by maintaining the PIL to LiFSI salt molar ratio to 1.5, higher ionic conductivity and a high Li ion transference number was achieved which highlights the significant influence of the cationic group within the PIL on the distribution of LiFSI salt. The co-coordination of FSI anions by both the polycation N^+ and Li^+ ions facilitate the dissociation of Li-FSI into Li^+ and FSI^- ions, with the highest content of PDADMA-FSI-Li achieved at a 1.5 ratio of polycation N^+ to LiFSI salt, resulting in a Li^+ transference number of 0.56 [65].

Establishing efficient transport networks for both ions and electrons within a cathode is a fundamental prerequisite for enhancing energy density. For ASSLBs, the integration of SPEs into catholyte serves to establish a proficient ionic transfer network [66, 67]. However, the inherent electron-insulating properties of SPEs can impede electronic conductivity, necessitating careful design of the cathode composition to strike a balance between ionic and electronic conductivity. It is noteworthy that ongoing research not only focuses on enhancing the ionic conductivity of SPEs but also places significant emphasis on improving their interfacial compatibility with electrodes to enhance overall SPE-catholyte functionality. A novel polymer matrix can be engineered by incorporating various functional groups, each serving a distinct purpose. One functional group can be tailored to enhance room-temperature ionic conductivity, while another can be optimized for superior electrochemical performance and long-term stability. This approach presents the potential to create advanced SPEs for efficient catholyte.

Active Material (AM) and Electrically Conducting Additives (CA)

One of the key challenges in advanced ASSLBs is achieving higher energy density by increasing catholyte thickness on current collector film in which microstructure and mass ratio of active material as well as SPEs should be optimized for maximizing ionic conduction and energy density [68–70]. The proportion of AM in catholyte significantly affect the electrochemical performance of ASSLBs. Altering the solid polymer electrolyte (SPE) content in catholytes based on PEO-LiTFSI between 10 and 30% had a notable effect on electrochemical performance. With 15% of SPE in catholytes, the battery exhibited an average discharge capacity of 155 mAh g^{-1}. Further reduction in SPE content decreased the ionic pathways and resulted in decreased average discharge capacity [39]. It is noteworthy that SPEs adhere better to the active cathode materials comparing with traditional LEs, allowing for the preparation of homogeneous catholytes without significant challenges. For Example, a process involving cold calendaring after hot extrusion of a PEO-based electrolyte, lithium manganese oxide (LMO), and Super C65 carbon resulted in 100 µm thick films with minimal porosity and high mass loading (~ 15 mg cm^{-2}) [71].

The energy density of the cell is determined by the loading level of AM in the catholytes. When comparing two ASSLBs with identical cell configurations but different AM loadings of 6.05 and 12.0 mg cm^{-2}, they exhibited initial discharge capacities of 157.7 and 137.0 mAh g^{-1}, respectively. Both batteries achieved around 93% capacity retention after 160 and 129 cycles, respectively [39]. In certain instances, moderate cycling stability is observed with high loading of catholytes. For example, the Li/PVDF-HFP-LiTFSI-LLZTO/NMC532 solid-state battery with a loading of 10.5 mg cm^{-2} exhibited a specific discharge capacity of 146.9 mAh g^{-1} at 0.1 C, retaining 87% of its capacity after cycling [72]. Furthermore, the size of AM should be also carefully controlled as it influences the fabrication process as well as the electrochemical performance.

Electrically conducting additive (CA) is another essential component for composite cathode, ensuring efficient electron transport and uniform current distribution. CAs not only enhance electrode processability but also reduce polarization, ultimately improving the charging, discharging efficiency, and the lifespan of the batteries. The order and spatial distribution of conductive additives during cathode preparation directly impact the charge transfer and overall performance during the ASSLBs operation [73]. Since lithium ions are not stored in CA, their presence should be minimized as long as electronic conductivity reaches saturation value in the cathode [55, 74]. The relationship between electronic conductivity and the amount of CA in the cathode follows a percolation model, which suggests that there is a threshold of CA needed to achieve optimal conductivity [71]. In addition to regulating the mass ratio, the morphology of additives also significantly affects electronic conduction and interfacial reactions. For instance, while graphite and carbon nanoparticles (carbon black) require significantly high loading to achieve the percolation network, resulting in poor processibility, carbon nanotubes, graphene, and 3D carbon networks emerge as promising conductive additives due to their large surface area, flexibility, and porosity [75, 76]. Moreover, the functional groups in the CAs should be carefully selected because oxygen-containing groups in additives may cause side reactions leading to unstable interfaces [77]. To address the problem, a polymer layer on CAs can prevent side reactions and ensure fast electron transport for long-term stability in ASSLBs [78].

Interface and Stability

For high-performance ASSLBs, it is important to guarantee the mechanical, thermal, chemical, and electrochemical stability of the components and ensure their compatibility with the catholytes. ASSLBs must operate reliably across a wide voltage range, requiring solid polymer electrolytes (SPEs) capable of withstanding oxidation and reduction reactions. Therefore, it is crucial to carefully engineer the interfaces between the SPE, AM, and CA in the design of catholyte systems (Fig. 3a) [79]. One of the most critical challenges arises from the limited contact area between the catholyte's components, coupled with constrained ion transport pathways. This limitation results in a low utilization of active materials leading substantial loss of capacity and energy density in ASSLBs [80]. In addition, poor interface generates significant interfacial resistance, particularly during volume changes in the AM due to ion insertion/extraction. This resistance hampers ion migration and negatively affects battery performance [81, 82].

In case of ASSLBs incorporating catholytes (Fig. 3b), it is imperative that all interfaces in composite cathode including current collector must exhibit intimate connections as well as high stability. The intrinsic electrochemical instability of functional groups such as C–O, C=O, and C–H can cause the catholyte/SPE interface to become unstable, resulting in voltage polarization and capacity degradation [97]. SPE stability can be compromised by oxygen species generated at the interface during cycling, which becomes more critical at higher potentials or when the battery is operated at higher temperatures [98]. The highly catalytic nature of oxygen species originating from the $LiCoO_2$-catholytes is the primary cause of incompatibility with PEO-based ASSLBs, especially when charged to high voltages. This incompatibility is not solely attributed to the narrow thermodynamic electrochemical window of the PEO but is further exacerbated

by the presence of these oxygen species [99]. These issues can be addressed by the incorporation of Li salt additives to form a protective layer on the surface of composite cathode, which diminishes interfacial reactions between catholytes and SPE, ensuring enhanced overall performance and durability [100]. In another approach, surface coating of AM with polymer emerges as an effective strategy to establish a stable interface in catholytes and suppress the oxidation decomposition of the SPE [101]. For further enhancement, a robust anti-oxidant polymer material has been employed as a coating agents in the catholyte, effectively inhibiting side reactions and mitigating volume changes during operation [102]. For example, poly(ethyl cyanoacrylate) (PECA) was applied as buffer layer on the surface of $LiCoO_2$ through an in-situ polymerization, enhancing the interface stability between $LiCoO_2$ and the PEO. This improvement is attributed to the strong interaction between the lattice O^{2-} or Co^{3+} ions and electron-withdrawing groups (CO or CN) within PECA. Consequently, PEO is less susceptible to oxidation by $LiCoO_2$ at high charge potentials, ensuring a more stable and reliable battery performance [52].

Multilayer SPE can be another effective approach to establish stable interface contacts between the electrodes and the electrolyte in ASSLBs. A cost-effective double-layer polymer solid electrolyte can be designed to incorporate both features. In this matrix, the high anti-oxidation ability of poly(*N*-methyl-malonic amide) (PMA) ensures a stable catholyte/SPE interface. On the other hand, poly(ethylene oxide) with strong mechanical strength and high anti-reduction capability helps establish a stable anode/SPE interface while inhibiting the growth of Li dendrites. Moreover, double-layered flexible polymer electrolytes, when conformally adhered without any noticeable gap, have the potential to facilitate continuous ion migration across the polymer/polymer interface in the solid state. This contributes to improved battery performance and safety [104].

Electrochemical stability is defined by the voltage difference between the oxidation and reduction potential of an electrolyte, a parameter known as the electrochemical stability window (ESW). In simpler terms, it measures the energy difference between the highest occupied molecular orbital (HOMO) and the lowest unoccupied molecular orbital (LUMO) within the electrolyte. This parameter is crucial in assessing the performance of battery as it signifies the limit of the resistance in electrolyte to both oxidation and reduction processes. The LUMO represents the lowest energy level at which the electrolyte can accept electrons, while the HOMO is the highest energy level at which it can donate electrons [105, 106]. Numerous factors can reduce the electrochemical and chemical stability of ASSLBs. These include side reactions between the AM and SPE, oxidation decomposition of the SPE, dissolution of transition metal ions, and the aging or evolution of the interface during extended charge-discharge cycles (Fig. 3c) [19, 107, 108]. By employing a SPE-catholyte with an extended ESW, it becomes feasible to design high-voltage ASSLBs [109]. This expansion in ESW broadens the potential applications of SPEs, owing to their elevated energy density. These enhanced electrochemical and chemical stabilities are generally attributed to kinetic stabilizations rather than inherent thermodynamic characteristics. In simpler terms, it means that the observed exceptional stability is a result of how the reactions proceed over time rather than the inherent properties of the catholytes. The slower kinetics of decomposition reactions often lead to higher overpotential, which is a term used to describe the extra energy required to initiate these reactions [110, 111]. The nominal ESW is attributed to the higher overpotential associated with sluggish reaction kinetics. One of the ways to enhance the EWS of catholytes is by selecting appropriate Li salts which can also significantly improve the overall electrochemical properties of SPEs and compatibility with high voltage. For instance, SPE based on poly(ethylene glycol diacrylate), incorporating LiTFSI and lithium bisborate (LiBOB), has demonstrated a notable electrochemical stability window (ESW) ranging from 0 to 4.5 V vs. Li^+/Li. In this configuration, LiBOB serves to protect the current collector, while LiTFSI helps alleviate the reaction between LiBOB and Li metal. LiBOB also contributes to stabilizing the SPEs by suppressing the reduction reaction at a high overpotential [112].

For the SPE within composite electrodes, it is more crucial to consider the chemical stability or side reaction since it comes into contact with a large surface area of active materials while the focus has mainly been on assessing the mechanical stability of SPE between electrodes [113, 114]. In particular, the strong interactions between metal ions and oxygen, which can be released by certain active materials, may lead to significant side reactions particularly at the presence of SPE in composite cathodes [98]. The side reaction at the interfaces between AM and SPEs may result in the loss of AM in catholyte, the consumption of SPEs which may result in increasing internal resistance within the battery [79, 115].

Additionally, high-voltage ASSLBs with composite cathode can achieve high energy density which is comparable to that of commercial LIBs with liquid electrolytes. Nevertheless, Li dendrites frequently develop on the lithium metal anode in ASSLBs, posing a risk of short circuits and diminishing cycling stability along with other properties. To mitigate the formation and growth of lithium dendrites, the solid electrolyte should either be mechanically stronger than lithium metal or possess sufficient elasticity to accommodate structural changes caused by lithium dendrites [116]. Table 2 summarizes electrochemical stabilities and capacities of LMBs based on LE and SPEs. While typical SPEs are not mechanically stronger enough to effectively inhibit

Table 2 Cell configuration, capacity and electrochemical stability of liquid and solid polymer electrolytes in LIBs

Cell configuration	Electrolyte	Temp (°C)	Voltage (*V*)	Capacity/C-rate/retention% (cycles)	References
Liquid electrolytes (LEs)					
Li/Electrolyte/LFP	1:2.5 LiFSI/SL	30	3.8	160 mAh g^{-1}/0.5 C/92.7% (140)	[83]
Li/Electrolyte/LFP	LiFSI:DME:TTE = (1:0.58:4.92 by wt.)	30	4.2	105 mAh g^{-1}/4.20 mA cm^{-2}/~100 (500)	[84]
Li/Electrolyte/NCM 811	1 M LiFSI DME/TFEO (1.2 : 3 by mol.)	5	4.4	~ 175 mAh g^{-1}/2 C/80% (300)	[85]
Li/Electrolyte/NCM 622	10 m LiFSI EC/DMC	–	4.6	~ 237 mAh g^{-1}/–/86% (100)	[86]
Li/Electrolyte/LCO	LiTFSI–triglyme (1 : 1 by mol)	30	4.2	130 mAh g^{-1}/(1/8 C)/77% (200)	[87]
Li/Electrolyte/LCO	LiFSI–2TEP (1 : 2 by mol.) + 5% FEC + 0.05 M LiBOB	–	4.3	135 mAh g^{-1}/2 C/88% (350)	[88]
Solid polymer electrolytes-catholyte					
Li/Electrolyte/LFP	LiFSI/PEC (20 wt%)	30	5	120 mAh g^{-1}/0.05 C/–(1)	[44]
Li/Electrolyte/LFP	LiFSI/P (VDF-HFP) + PGCN (10 wt%)	26	4.45	92 mAh g^{-1}/0.5 C/71% (400)	[89]
Li/Electrolyte/NCM 111	LiFSI/P (DADMA) FSI ($DADMA^+$/Li^+ = 2:3)	80	5	130 mAh g^{-1}/0.06 C/–(50)	[65]
Li/Electrolyte/NCM 532	LiFSI/PVEC (16 wt%)	25	5.3	95 mAh g^{-1}/2 C/79.4% (200)	[90]
Li/Electrolyte/LCO	p-LPSCl/P(PEGMEA)	45	> 4.5	133 mAh g^{-1}/0.2 C/84% (90)	[91]
Li/Electrolyte/LCO	CPL(CA/PEG/LiTFSI + LATP)	60	5	157 mAh g^{-1}/0.5 C/~98% (100)	[92]
Solid polymer electrolytes (SPEs)-catholyte (CC)					
Li/SPE/LFP-CC	SPE = 90LLZTO-10PEO_{18} CC-55 wt% $LiFePO_4$, 20 wt% LLZTO powder, 10 wt% Super-P, and 15 wt% PEO-LiTFSI	60	5.2	151.6 mAh·g^{-1}/0.1 C/97.8% (50)	[93]
Li/SPE/LFP-CC	SPE = LiFNFSI/PEO CC-$LiFePO_4$ powder: Super P: SPEs: PVDF = 65:10:20:5(wt%)	80	5.45	–/1 C/80.8% (570)	[94]
Li/SPE/NCM-CC	SPE = PVDF/PAA/LiFSI CC = NCM:PEO:LiTFSI:superP = 76: 10:4:10 (wt%)	30	4.3	–/88 µA cm^{-2}/98.5% (160)	[95]
Li/SPE/NCM811-CC	SPE = LiTFSI-PEO-0.2AlF_3 CC = NCM: carbon black:PEO:LiTFSI 60:12:20:8 (wt%)	60	5.3	200 mAh g^{-1}/–/–(900)	[96]
Li/SPE/LCO-CC	SPE = PVDF-LiFSI/PAA(3wt%) CC-$LiCoO_2$: PEO:LiTFSI:super *P* = 79:12:4:5 (wt%)	30	4.64	80/88 µA cm^{-2}/0.0.3% decay per cycle (1000)	[95]

the growth of Li dendrites, the composite SPE can tolerate larger strains and have been shown to enhance cycling stability (Fig. 3d) [31]. Alternatively, polymers can be crosslinked or inorganic fillers can be introduced for mechanically much stronger SPE-catholyte [113, 114]. Recently, a membrane-supported solid polymer electrolyte (SPE) was reported as an effective strategy to enable the use of SPEs in high-voltage ASSLBs, showcasing commendable cycling performance and improved safety [50].

In more harsh condition, battery become thermally unstable resulting in the high interfacial resistance, which may trigger thermal runaway during charging and discharging processes [117, 118]. In addition to SPE and CA in catholytes, flame-retardant components are incorporated as shown in Fig. 3e. Zinc hydroxystannate, along with grafting ionic-conductive PEA in catholyte system has proven to be highly successful in enhancing both thermal stability and mechanical strength [103]. Abels et al. combined PEO with three different salts which reduced the combustion temperature of pure PEO. The addition of Li salts resulted in exothermic signals during the decomposition process, and LiTFSI and LiBETI salts exhibited better thermal stability compared to $LiClO_4$. Furthermore, their findings indicated that catholytes with lithium nickel manganese cobalt oxides (NMC) can react with thermally degrading PEO or fluorine radicals, leading to the formation of oxygen and subsequent combustion of the SPE. The influence of catholytes- AM on the thermal stability of SPEs revealed that higher NMC ratios

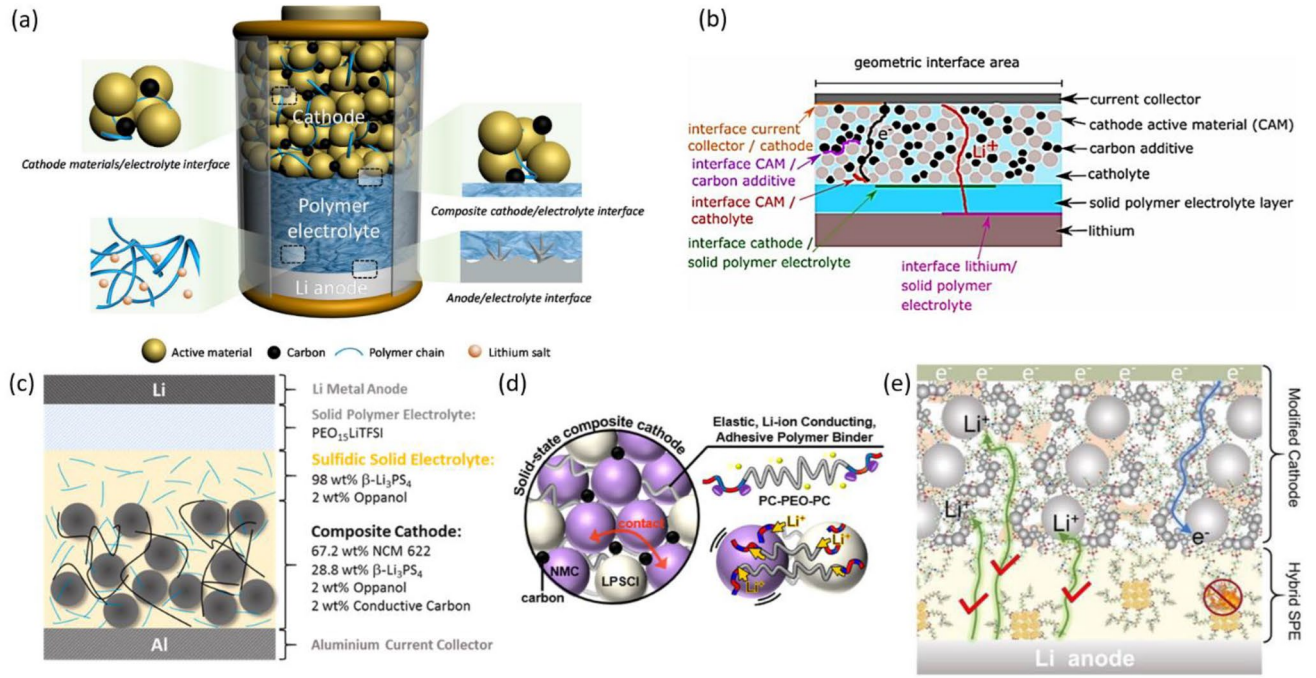

Fig. 3 Schematic representations of **a**, **b** interfaces generated by SPE and catholyte integration. Adapted from ref. [79]. copyright 2021 Elsevier and Adapted from ref. [97]. under the terms of the Creative Commons Attribution 4.0 License (CC BY, http://creativecommons.org/licenses/by/4.0/) copyright 2019 IOP, respectively **c** double-layered films with polymer and sulfide-based solid electrolytes. Adapted from ref. [19]. copyright 2019 Elsevier **d** ABA triblock polymers of poly(4-vinyl cyclohexene oxide carbonate) and PEO in catholyte featuring mechanical rigidity and enhances oxidative stability. Adapted from ref. [31]. under the terms of the Creative Commons Attribution 4.0 License (CC BY, http://creativecommons.org/licenses/by/4.0/) copyright 2022 American Chemical Society and **e** ASSLB with catholyte with poly(ether amine)-coated zinc hydroxystannate (PEA@ZHS) for thermal stability. Adapted from ref. [103]. copyright 2022 Elsevier

generated more oxygen, leading to more intense combustion reactions and higher enthalpies within the PEO electrolytes [119].

Electrochemical Transportation in Catholytes

In ASSLBs, electrochemical transport is hindered by interface resistances and morphology of electrode that limit fast charging and discharging. Therefore, it is most important to establish effective ion transport networks with minimal SPE in catholytes for high-energy-density ASSLBs, which requires careful evaluation of compositions, structure, and particle size distribution. Furthermore, to enhance ion transport in catholytes, several physicochemical parameters should be carefully considered which include salt dissociation, interactions between cations and polymer chains, solvation structures, coordination number of solvation, and glass transition temperature (T_g) [81, 120, 121]. Moreover, porous structure also plays a crucial role in the ion transport mechanism in catholytes. Like the 3D structure not only increased loading levels but also exhibited better areal capacity compared to 2D electrodes, due to continuous SPE structures and SPE/electrode interfacial compatibility, resulting in excellent ionic conductivity and electrochemical stability. For example, ion transport in catholytes can be greatly enhanced by implementing multilayer or interpenetrating structures within them. Zhang et al. demonstrated a 3D porous $Li_{1.5}Al_{0.5}Ge_{1.5}(PO_4)_3$ (LAGP) layer with NCM as catholyte, which are assembled with LAGP layers and SPE-coated lithium metal layers of anode [122].

Ionic (σ_i) and Electronic (σ_e) Conductivity

In ASSLBs, SPE are specifically used to establish an efficient ionic transfer network. However, their inherent electron-insulating properties hinder overall conductivity [123, 124]. In SPE, Li^+ ions are conducted via segmental relaxation, primarily by coordinating with oxygen atoms along the polymer chain's backbone, forming complexes with alkali-metal cations. Ionic conduction takes place above the glass transition temperature (T_g) within the amorphous phase of the polymer [125]. Through sub-diffusive motion, intersegmental hopping and collective motion involving the entire polymer chain and coordinated ions, Li^+ ions transverse

along the polymer chain. In high-molecular-weight polymers, intersegmental hopping becomes the dominant mechanism for ionic conduction as entangled chains play a major role in solvating ions [126]. In contrast, low-molecular-weight polymers and oligomers primarily rely on ion diffusion in their solvated form, similar to the behavior observed in carbonate-based liquid electrolytes [127].

In catholytes, both ionic (σ_i) and electronic (σ_e) conductivities can be optimized by engineering the structures of the catholytes [66, 128]. High concentrations of mobile ion carriers and low activation energies result in high conductivities. The Arrhenius model effectively explains the behavior of both polymers and solid ion conductors in terms of σ_i [129].

$$\sigma_i = \frac{\sigma_0}{T} e^{-E_A/k_B T},$$

where E_A represents the activation energy of migration of the ions, T indicates temperatures in Kelvin, k_B represents Boltzmann's constant, and σ_0 represents the pre-exponential factor (including the entropy of migration and the charge carriers). Ion conductivity (σ_i) in SPEs can also be explained by other models, including the Vogel–Tammann–Fulcher model, which considers the continuous motion and relaxation of the polymer backbone to explain non-linear log σ_i vs. $1/T$ graphs. Ion transport in SPEs is thus affected by its fraction of mobile ions n_i, its number of ions mobilized u_i, its size and its charge q_i, as well as its intrinsic characteristics, according to the equation below [129].

$$\sigma_i(T) = \sum_i n_i q_i u_i,$$

When symmetric cells with ion-blocking electrodes [stainless steel SS|SPE|SS] are used, it is easy to determine the ionic conductivity (σ_i) of SPEs using EIS (Fig. 4a) [130, 131]. The configurations equivalent circuit comprised of bulk resistance (R_{bulk}) and double-layer capacitance in series along with geometric capacitance in parallel [129]. The ionic conductivity is given by $\sigma_i = L/(S \cdot R_{bulk})$, where L and S are the electrode area and electrolyte thickness, respectively. When dealing with catholyte, it can be challenging to determine the effective ionic resistance using conventional EIS analysis with the ion-blocking cell configuration due to its electronic conductivity. While ionic conductivity (σ_i) has received significant attention in the context of LIBs, an equal consideration should be given to electronic conductivity (σ_e). To ensure rapid charge and discharge, ideally, σ_e should exceed 1.0 S cm^{-1} [132]. Low σ_e of SPE helps prevent short circuits and conductivity enhancers (carbon black) are typically incorporated into catholytes for electronic percolation.

As an alternative to EIS, direct current (DC) polarization with ion- (SS|catholyte|SS) and electron- (Li|SPE|catholyte|SPE|Li) blocking symmetric cells can be used to determined σ_e and σ_i, respectively (Fig. 4b and c). The equilibrium current of the ion-blocking cell represents an electronic current under DC polarization, indicating no ion migration. Similarly, the equilibrium current of the electron-blocking cell indicates an ionic current without electron conduction. Recently, to quantitatively evaluate the structural connectivity and ionic property of the ion transporting network in catholyte, another EIS analysis using a catholyte symmetric cell configuration (SS|SPE|catholyte|SPE|SS) has been reported (Fig. 4d) [131]. While there is no liquid in ASSLBs, the predominant conduction mechanism is ionic migration rather than diffusion. Utilizing fluid-like properties in catholytes, the Nernst–Einstein equation is employed to characterize the relation of the lithium diffusion coefficient $D^{ion}_{bulk,\,SPE}$ and ionic bulk conductivity of the SPE $\sigma^{ion}_{bulk,SPE}$.

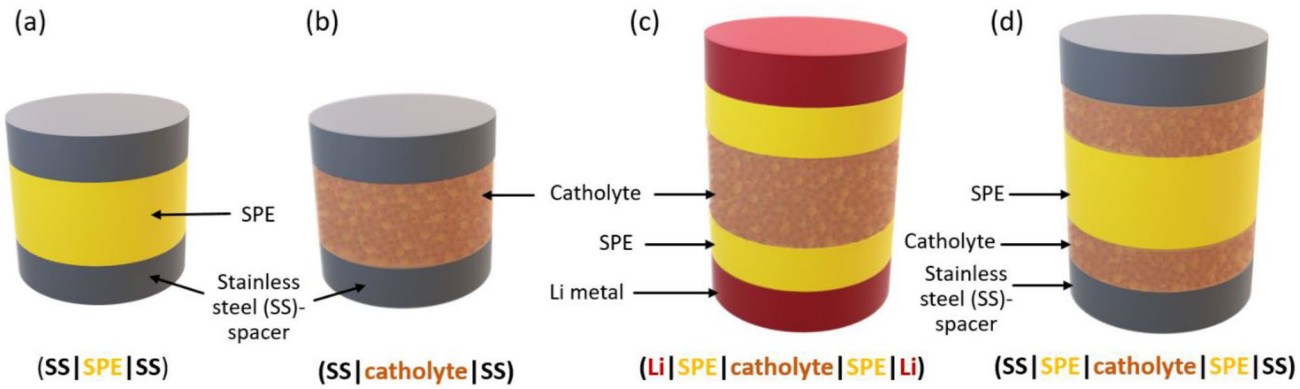

Fig. 4 Schematic representations of **a** conventional ion-blocking cell with SPE, **b** ion- and **c** electron-blocking cell with catholyte, and **d** catholyte symmetric cell

$$D_{\text{eff}}^{\text{ion}} = \frac{\varepsilon}{\tau^2} D_{\text{bulk}}^{\text{ion}} = \frac{\varepsilon}{\kappa} D_{\text{bulk}}^{\text{ion}},$$

$$D_{\text{bulk, SPE}}^{\text{ion}} = \frac{\sigma_{\text{bulk,SPE}}^{\text{ion}} RT}{c_{\text{bulk,SPE}}^{\text{ion}} F^2},$$

The effective ionic conductivity and ion transport tortuosity of the catholyte can be determined by the $\sigma_{\text{eff}}^{\text{ion}}$ and R_{ion}.

$$\sigma_{\text{eff}}^{\text{ion}} = \frac{\varepsilon_{\text{SPE}}}{\tau^2} \sigma_{\text{bulk,SPE}}^{\text{ion}},$$

where ionic diffusion of bulk material ($D_{\text{bulk}}^{\text{ion}}$), porosity ($\varepsilon$), tortuosity factor ($\kappa$) and tortuosity ($\tau$) are quantification of huddles to Li^+ ion transport within a microstructure due to interconnected insulating phases, like pores. R, T and F are gas constant, absolute temperature and Faraday's constant, respectively. By the transmission line model (TLM) without faradaic reactions, the ion transport resistance in the catholyte (R_{ion}) can be estimated for the low frequency limit of the real part impedance of the catholyte symmetric cell.

$$Z'_{w\to 0} = R_{\text{electrolyte}} + \frac{1}{3} R_{\text{ion}},$$

where $R_{\text{electrolyte}}$ denotes the ionic resistance of additional electrolyte. Furthermore, τ can be defined as the ratio of the shortest path through the microstructure to its overall length. Catholytes, which also exhibit high tortuosity, directly influence the effective ionic conductivity. Alternatively, in a symmetrical cell with a Li^+ blocking configuration (Fig. 4b), τ information can be obtained using EIS [133, 134]. Trembacki et al. calculated τ by performing 3D reconstruction of X-Ray tomography data. Additionally, focused ion beam scanning electron microscopy (FIB-SEM) can be employed for τ calculations [135, 136].

Lithium-ion Transference Number (t_{Li}^+)

The contribution of Li^+ ions to the conductivity can be determined from the mobilities of cations and anions (ideally t_{Li}^+=1). To calculate t_{Li}^+, the Hittorf method is used, in which ion concentration changes near the electrodes are measured, along with changes in electrolyte solution concentration. An EIS and DC polarization experiment with electron blocking electrodes are typical methods for investigating charge transport in mixed-conducting systems (Fig. 4c). Choosing the electrode material is critical since it connects the sample to the EIS system. A low-frequency barrier should be either ionically or electronically insulated, e.g. stainless steel or Li_6PS_5Cl (LPS-Cl) [122]. To measure the t_{Li}^+ AC impedance is obtained by chronoamperometry method where cells are combined as Li/SE/Li [137].

$$t_{Li^+} = \frac{I_s(\Delta V - I_0 R_0)}{I_0(\Delta V - I_s R_s)},$$

where ΔV is the polarization with a voltage, I_0 and I_s are the initial and steady-state current, R_0 and R_s are the initial and steady-state resistance.

Preparation Techniques of Catholytes

Catholytes can be fabricated using a variety of techniques because there is no universally optimized method that can work effectively for all battery chemistries. As a primary consideration when selecting the processing method, the physical and chemical characteristics of the SPEs used must be considered [138]. The preparation of ASSLBs with catholyte is often experimented with different methods of preparation. Some techniques, however, are more commonly used than others. Like, SPEs are used to prepare catholyte using the slurry coating method. In this approach, SPE, AM and CA are blended in a solvent and then applied to the substrate before evaporating the solvent (Fig. 5a). It is, however, very difficult to completely dry the remaining traces of solvent with this technique. Lithium salt in catholyte can react with residual solvent, resulting in interfacial instability [10, 17, 57, 139]. Even then, slurry coating is more versatile than dry blending because many polymers in SPEs are chemically stable and highly soluble in specific solvents (Fig. 5b) [140]. This method was used by Fan et al. to develop a catholyte containing PVDF, succinonitrile (SCN), and LiTFSI at a loading of 10.5 mg cm^{-2}. It delivers capacity of 146.9 mAh g^{-1} and retains 86.89% of its capacity even after 150 cycles at a 0.1 C rate [72]. The slurry infiltration method can also be used to make catholytes. Through this method, SPE slurry is applied directly to the dried cathode, which has porous or designed structures. By freeze–drying an LFP electrode, Yang et al. achieved a high loading of 10.5 mg cm^{-2}. The electrode micro gaps were filled with catholyte (LiTFSI/PEO) solution. This smart design allows for high active material utilization and stable cycling with an area capacity of 1.52 mAh cm^{-2} [141].

Hot/cold pressing is an environmentally friendly method that does not involve toxic solvents. When making catholyte using SPEs, the process typically includes mixing the SPE, AM and CA in mills or by chop-chopping (Fig. 5a) [142]. Then, these materials are hot pressed or extruded at high temperatures, followed by rolling calendaring. Linear polymers become highly viscous and low fluid above their melting point (typically above 60 °C) which is beneficial for good dispersion and uniform mixing. For hot pressing, PEO is well suited because of its low melting point. For example, Wetjen et al. used a ratio of 43:7:17.5:5:27.5 order to create a catholyte consisting of LFP, CA, PEO, LiTFSI,

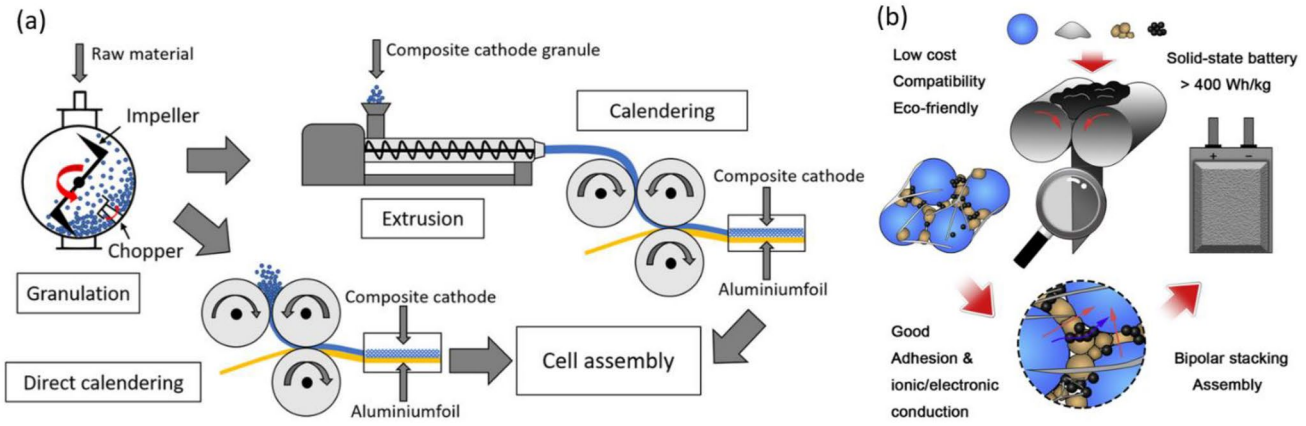

Fig. 5 Catholyte fabrication techniques **a** process chain for slurry coating method and milling or chop-chopping. Adapted from ref. [142]. Copyright 2022 John Wiley and Sons and **b** schematic illustration of dry battery electrode (DBE). Adapted from ref. [140]. Copyright 2022 Elsevier

and Pyr14TFSI [16]. Whereas uniaxial cold press technique (300–500 MPa) was used to make catholyte pellets for ASSLBS. Furthermore, similar technique known as dry blending, involves high shear forces and temperatures that can break polymer macromolecule chains, affecting the polymer's mechanical and adhesive properties. Therefore, it's crucial to optimize factors such as rotation speed, cycle time, processing temperature, and extrusion and hot-pressing times [71].

Polymerization is an effective approach that ensures close interaction between various components in catholyte, facilitating ion transport and optimizing active material utilization. This technique simplifies the catholyte fabrication process and is highly compatible with current production lines. There are many advantages to incorporating in-situ polymerization, including enhancing interfacial compatibility, preventing transition metal ions from dissolving, cautioning lithium dendrite growth, and enhancing the overall performance of the battery. For example, a 600 µm thick cathode with vertically aligned NMC811-rich pillars surrounded by ionic SPE was fabricated in a single step using a directional freezing and polymerization (DFP) process. This process self-assembles active cathode particles and ionic SPE into a preferred catholyte structure without the need for additional steps like pressing, heating, solid-state electrolyte infiltration, or template removal. The DFP method achieves an intimate interfacial contact, resulting in a cathode with a near-theoretical gravimetric capacity of 199 mAh g^{-1} and an ultra-high areal capacity of 16.7 mAh cm^{-2} at 0.05 C, and 120 mAh g^{-1} (10.1 mAh cm^{-2}) at room temperature. This performance is among the highest reported under the same testing conditions [143].

A composite cathode is formed using two sequential steps in in-situ polymerization. Precursor suspensions consist of solid polymer electrolyte (SPE) precursors, active materials, lithium salts, crosslinking agents, initiators, and other agents, followed by the preparation of a precursor suspension. Afterwards, polymerization takes place by irradiation or thermal means. As an example, Zhang et al. used LFP, carbon black, poly(ethylene glycol) diacrylate, and a photoinitiator to prepare a precursor suspension. To produce the catholyte, the suspension was coated on aluminum foil, then UV polymerized and dried. Compared to traditional coin cells, the resulting coin cell exhibited superior cycling performance when an in-situ catholyte and lithium metal were combined [144].

Summary and Perspectives

ASSLBs stand out as promising candidates for future energy storage. Despite their potential, critical challenges persist, particularly concerning the interfacial contact between solid electrolytes and electrodes, and the low ion or electrical conductivity within thick cathodes which is essential for achieving high energy density. To address interfacial contact issues, SPE particles have been incorporated into cathode layers, forming a composite cathode or catholytes. This not only enhances interfacial contact but also establishes ion conduction pathways within the cathodes, allowing for the design of thicker cathode layers and, consequently, achieving higher energy density. Tailoring the intrinsic properties of SPEs significantly enhances catholyte utilization, particularly in terms of mechanical stability, the electrochemical stability window, and electrochemical transport kinetics. However, ongoing research on catholyte ASSLBs faces challenges such as high voltage operation, stable catholyte interfaces, unwanted side reactions, the density of efficient ion-conducting pathways at room temperature, and the occurrence of volume changes during cycling, voids, and cracks at interfaces.

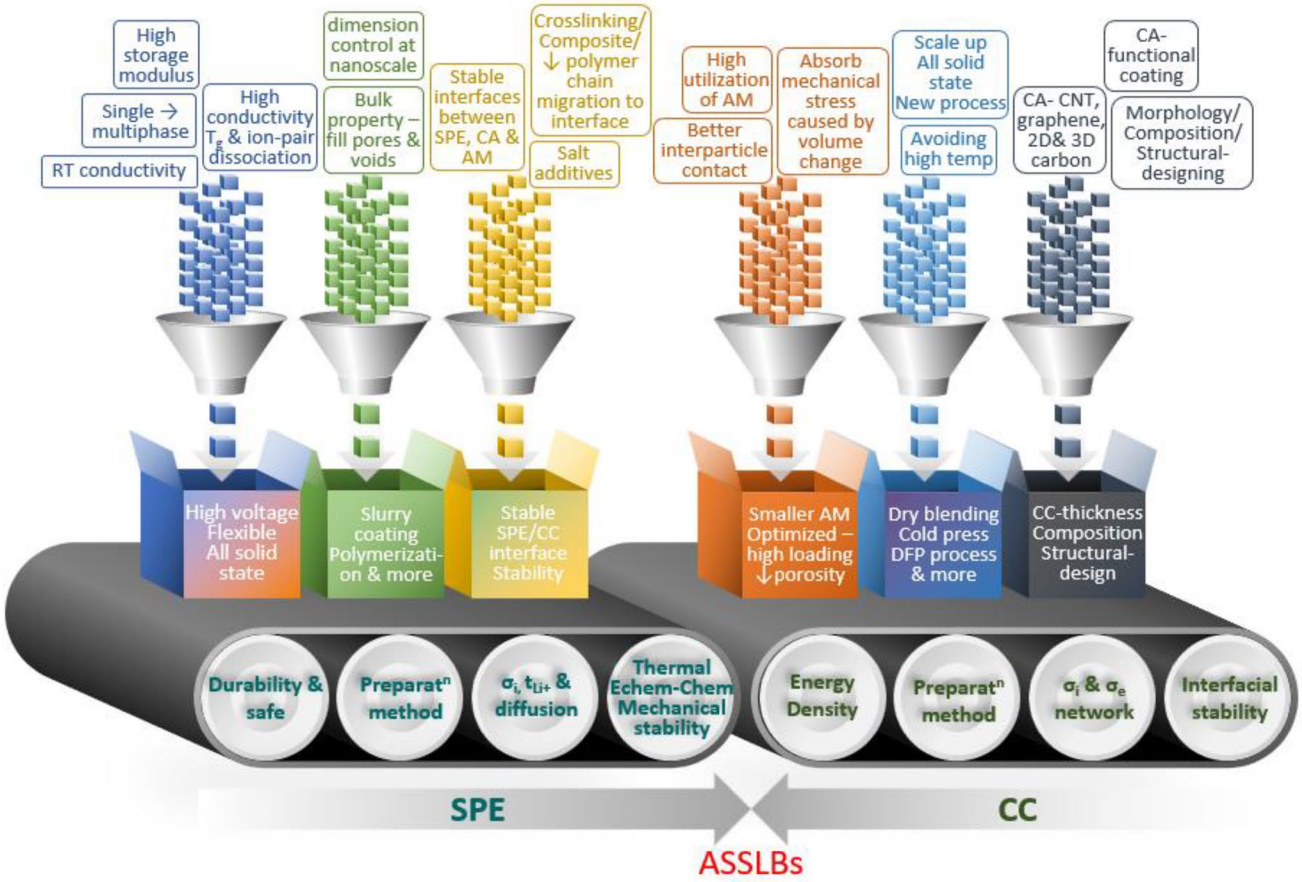

Fig. 6 Schematic illustration of challenges and corresponding solutions to attain high-performance ASSLBs based on catholyte

These challenges can be effectively addressed through the incorporation of various functional groups, careful material selection, innovative structural design, and other strategies (see Fig. 6).

In the future, concerted efforts should be directed toward overcoming issues related to poor interface contacts, large interfacial resistance, and inferior interface compatibility in catholytes. The introduction of catholytes in ASSLB assembly eliminates the need for a separator, and when combined with recent bipolar design techniques for composite cathodes, it has the potential to enhance energy density by reducing the current collector requirement. Adopting such approaches for catholyte systems in ASSLBs represents a significant stride towards their commercialization.

Author Contributions Literature review, wrote the original manuscript and image-table organization layout and obtained copyright licenses: UK and KPS. Reviewing and editing: W-JC, S-KC, J-JH. Conception, supervision and reviewing: G-RY.

Data Availability Not applicable.

Declarations

Conflict of interest All authors declared that there are no conflicts of interest.

Financial Support and Sponsorship This research was supported by Creative Materials Discovery Program through the National Research Foundation of Korea (NRF) funded by Ministry of Science and ICT(2018M3D1A1058624) and LG Energy Solutions.

References

1. Y. Jin, B. Zhu, Z. Lu, N. Liu, J. Zhu, Adv. Energy Mater. **7**, 1700715 (2017)
2. W. Xu, J. Wang, F. Ding, X. Chen, E. Nasybulin, Y. Zhang, J.-G. Zhang, Energy Environ. Sci. **7**, 513 (2014)
3. X.B. Cheng, C.Z. Zhao, Y.X. Yao, H. Liu, Q. Zhang, Chem **5**, 74 (2019)
4. K. Deng, T. Guan, F. Liang, X. Zheng, Q. Zeng, Z. Liu, G. Wang, Z. Qiu, Y. Zhang, M. Xiao, Y. Meng, L. Wei, J. Mater. Chem. A **9**, 7692 (2021)
5. F. Han, Y. Zhu, X. He, Y. Mo, C. Wang, Adv. Energy Mater. **6**, 1501590 (2016)
6. S. Xia, X. Wu, Z. Zhang, Y. Cui, W. Liu, Chem **5**, 753 (2019)

7. S. Jian, Y. Cao, W. Feng, G. Yin, Y. Zhao, Y. Lai, T. Zhang, X. Ling, H. Wu, H. Bi, Y. Dong, Mater. Today Sustain. **20**, 100224 (2022)
8. B. Chen, Z. Huang, X. Chen, Y. Zhao, Q. Xu, P. Long, S. Chen, X. Xu, Electrochim. Acta **210**, 905 (2016)
9. Y.-K. Sun, ACS Energy Lett. **5**, 3221 (2020)
10. L. Chen, X. Qiu, Z. Bai, L.-Z. Fan, J. Energy Chem. **52**, 210 (2021)
11. R. Schlem, C.F. Burmeister, P. Michalowski, S. Ohno, G.F. Dewald, A. Kwade, W.G. Zeier, Adv. Energy Mater. **11**, 2101022 (2021)
12. A. Banerjee, H. Tang, X. Wang, J.-H. Cheng, H. Nguyen, M. Zhang, D.H.S. Tan, T.A. Wynn, E.A. Wu, J.-M. Doux, T. Wu, L. Ma, G.E. Sterbinsky, M.S. D'Souza, S.P. Ong, Y.S. Meng, ACS Appl. Mater. Interfaces **11**, 43138 (2019)
13. Y. Xiao, L.J. Miara, Y. Wang, G. Ceder, Joule **3**, 1252 (2019)
14. J. Guo, G. Ma, K. Hu, L. Song, X. Yan, Y. Gao, M. Zhang, Ionics **28**, 619 (2022)
15. T. Kato, S. Iwasaki, Y. Ishii, M. Motoyama, W.C. West, Y. Yamamoto, Y. Iriyama, J. Power Sources **303**, 65 (2016)
16. M. Wetjen, G.-T. Kim, M. Joost, G.B. Appetecchi, M. Winter, S. Passerini, J. Power Sources **246**, 846 (2014)
17. C. Xin, K. Wen, C. Xue, S. Wang, Y. Liang, X. Wu, L. Li, C.-W. Nan, Batteries & Supercaps **5**, e202100162 (2022)
18. L. Porcarelli, A.S. Shaplov, M. Salsamendi, J.R. Nair, Y.S. Vygodskii, D. Mecerreyes, C. Gerbaldi, ACS Appl. Mater. Interfaces **8**, 10350 (2016)
19. T. Ates, M. Keller, J. Kulisch, T. Adermann, S. Passerini, Energy Storage Mater. **17**, 204 (2019)
20. J. Li, J. Qi, F. Jin, F. Zhang, L. Zheng, L. Tang, R. Huang, J. Xu, H. Chen, M. Liu, Y. Qiu, A.I. Cooper, Y. Shen, L. Chen, Nat. Commun. **13**, 2031 (2022)
21. N.D. Trinh, M. Saulnier, D. Lepage, S.B. Schougaard, J. Power Sources **221**, 284 (2013)
22. D. Devaux, D. Glé, T.N.T. Phan, D. Gigmes, E. Giroud, M. Deschamps, R. Denoyel, R. Bouchet, Chem. Mater. **27**, 4682 (2015)
23. V.T. Luu, Q.H. Nguyen, M.G. Park, H.L. Nguyen, M.-H. Seo, S.-K. Jeong, N. Cho, Y.-W. Lee, Y. Cho, S.N. Lim, Y.-S. Jun, W. Ahn, J. Mater. Res. Technol. **15**, 5849 (2021)
24. I. Aldalur, H. Zhang, M. Piszcz, U. Oteo, L.M. Rodriguez-Martinez, D. Shanmukaraj, T. Rojo, M. Armand, J. Power Sources **347**, 37 (2017)
25. J. Chai, Z. Liu, J. Ma, J. Wang, X. Liu, H. Liu, J. Zhang, G. Cui, L. Chen, Adv. Sci. **4**, 1600377 (2017)
26. X. Zhang, S. Wang, C. Xue, C. Xin, Y. Lin, Y. Shen, L. Li, C.-W. Nan, Adv. Mater. **31**, 1806082 (2019)
27. J. Hu, P. He, B. Zhang, B. Wang, L.-Z. Fan, Energy Storage Mater. **26**, 283 (2020)
28. R. Bouchet, S. Maria, R. Meziane, A. Aboulaich, L. Lienafa, J.-P. Bonnet, T.N.T. Phan, D. Bertin, D. Gigmes, D. Devaux, R. Denoyel, M. Armand, Nat. Mater. **12**, 452 (2013)
29. Y.-C. Jung, S.-M. Lee, J.-H. Choi, S.S. Jang, D.-W. Kim, J. Electrochem. Soc. **162**, A704 (2015)
30. Z. Wan, D. Lei, W. Yang, C. Liu, K. Shi, X. Hao, L. Shen, W. Lv, B. Li, Q.-H. Yang, F. Kang, Y.-B. He, Adv. Funct. Mater. **29**, 1805301 (2019)
31. G.L. Gregory, H. Gao, B. Liu, X. Gao, G.J. Rees, M. Pasta, P.G. Bruce, C.K. Williams, J. Am. Chem. Soc. **144**, 17477 (2022)
32. J.-H. Choi, C.-H. Lee, J.-H. Yu, C.-H. Doh, S.-M. Lee, J. Power Sources **274**, 458 (2015)
33. Y.-C. Jung, M.-S. Park, C.-H. Doh, D.-W. Kim, Electrochim. Acta **218**, 271 (2016)
34. J. Zhang, X. Zang, H. Wen, T. Dong, J. Chai, Y. Li, B. Chen, J. Zhao, S. Dong, J. Ma, L. Yue, Z. Liu, X. Guo, G. Cui, L. Chen, J. Mater. Chem. A **5**, 4940 (2017)
35. Y. Zhao, Z. Huang, S. Chen, B. Chen, J. Yang, Q. Zhang, F. Ding, Y. Chen, X. Xu, Solid State Ion. **295**, 65 (2016)
36. P. López-Aranguren, X. Judez, M. Chakir, M. Armand, L. Buannic, J. Electrochem. Soc. **167**, 020548 (2020)
37. H. Al-Salih, A. Huang, C.-H. Yim, A.I. Freytag, G.R. Goward, E. Baranova, Y. Abu-Lebdeh, J. Electrochem. Soc. **167**, 070557 (2020)
38. X. Zhang, T. Liu, S. Zhang, X. Huang, B. Xu, Y. Lin, B. Xu, L. Li, C.-W. Nan, Y. Shen, J. Am. Chem. Soc. **139**, 13779 (2017)
39. R.-J. Chen, Y.-B. Zhang, T. Liu, B.-Q. Xu, Y.-H. Lin, C.-W. Nan, Y. Shen, ACS Appl. Mater. Interfaces **9**, 9654 (2017)
40. N. Pravin, Y.N. Didwal, R. Singhbabu, B.-J. Verma, G.-H. Sung, J.-S. Lee, D.R. Lee, C.-J. Chang, Park, Energy Storage Mater. **37**, 476 (2021)
41. Y. Son, H. Cha, C. Jo, A.S. Groombridge, T. Lee, A. Boies, J. Cho, M. De Volder, Mater. Today Energy **21**, 100838 (2021)
42. L. Yue, J. Ma, J. Zhang, J. Zhao, S. Dong, Z. Liu, G. Cui, L. Chen, Energy Storage Mater. **5**, 139 (2016)
43. C. Liu, F. Zhu, Z. Huang, W. Liao, X. Guan, Y. Li, D. Chen, Z. Lu, Chem. Eng. J. **434**, 134644 (2022)
44. K. Kimura, M. Yajima, Y. Tominaga, Electrochem. Commun. **66**, 46 (2016)
45. P.C. Barbosa, L.C. Rodrigues, M.M. Silva, M.J. Smith, Solid State Ion. **193**, 39 (2011)
46. J. Zhang, J. Zhao, L. Yue, Q. Wang, J. Chai, Z. Liu, X. Zhou, H. Li, Y. Guo, G. Cui, L. Chen, Adv. Energy Mater. **5**, 1501082 (2015)
47. Y. Xia, T. Fujieda, K. Tatsumi, P.P. Prosini, T. Sakai, J. Power Sources **92**, 234 (2001)
48. Y. Liang, S. Guan, C. Xin, K. Wen, C. Xue, H. Chen, S. Liu, X. Wu, H. Yuan, L. Li, C.-W. Nan, ACS Appl. Mater. Interfaces **14**, 32075 (2022)
49. C. Liu, R.L. Sacci, R. Sahore, G.M. Veith, N.J. Dudney, X.C. Chen, J. Power Sources **527**, 231165 (2022)
50. Y. Seo, Y.-C. Jung, M.-S. Park, D.-W. Kim, J. Membr. Sci. **603**, 117995 (2020)
51. C. Song, Z. Li, J. Peng, X. Wu, H. Peng, S. Zhou, Y. Qiao, H. Sun, L. Huang, S.-G. Sun, J. Mater. Chem. A **10**, 16087 (2022)
52. J. Ma, Z. Liu, B. Chen, L. Wang, L. Yue, H. Liu, J. Zhang, Z. Liu, G. Cui, J. Electrochem. Soc. **164**, A3454 (2017)
53. B. Sun, J. Mindemark, E.V. Morozov, L.T. Costa, M. Bergman, P. Johansson, Y. Fang, I. Furó, D. Brandell, Phys. Chem. Chem. Phys. **18**, 9504 (2016)
54. J. Zhang, J. Yang, T. Dong, M. Zhang, J. Chai, S. Dong, T. Wu, X. Zhou, G. Cui, Small **14**, 1800821 (2018)
55. L. Li, H. Duan, J. Li, L. Zhang, Y. Deng, G. Chen, Adv. Energy Mater. **11**, 2003154 (2021)
56. H. Duan, M. Fan, W.-P. Chen, J.-Y. Li, P.-F. Wang, W.-P. Wang, J.-L. Shi, Y.-X. Yin, L.-J. Wan, Y.-G. Guo, Adv. Mater. **31**, 1807789 (2019)
57. J.H. Yoon, W.-J. Cho, T.H. Kang, M. Lee, G.-R. Yi, Macromol. Res. **29**, 509 (2021)
58. J.H. Lee, J.C. Shin, J. Kim, J.-W. Ho, W.J. Cho, M.J. Park, G.-R. Yi, M. Lee, P.J. Yoo, J. Power Sources **557**, 232565 (2023)
59. W.-J. Cho, S.-K. Cho, J.H. Lee, J.H. Yoon, S. Kwon, C. Park, W.B. Lee, P.J. Yoo, M. Lee, S. Park, T.H. Kang, G.-R. Yi, J. Mater. Chem. A **11**, 1676 (2023)
60. Z.C. Zhang, J.J. Jin, F. Bautista, L.J. Lyons, N. Shariatzadeh, D. Sherlock, K. Amine, R. West, Solid State Ion. **170**, 233 (2004)
61. L. Miao, H. Duan, D. Zhu, Y. Lv, L. Gan, L. Li, M. Liu, J. Mater. Chem. A **9**, 2714 (2021)
62. R. Li, Z. Fang, C. Wang, X. Zhu, X. Fu, J. Fu, W. Yan, Y. Yang, Chem. Eng. J. **430**, 132706 (2022)
63. P. Guo, H. Zhang, X. Liu, J. Sun, ACS Appl. Mater. Interfaces **10**, 2105 (2018)

64. R. Rojaee, S. Cavallo, S. Mogurampelly, B.K. Wheatle, V. Yurkiv, R. Deivanayagam, T. Foroozan, M.G. Rasul, S. Sharifi-Asl, A.H. Phakatkar, M. Cheng, S.-B. Son, Y. Pan, F. Mashayek, V. Ganesan, R. Shahbazian-Yassar, Adv. Funct. Mater. **30**, 1910749 (2020)
65. X. Wang, F. Chen, G.M.A. Girard, H. Zhu, D.R. MacFarlane, D. Mecerreyes, M. Armand, P.C. Howlett, M. Forsyth, Joule **3**, 2687 (2019)
66. Y. Liang, H. Liu, G. Wang, C. Wang, Y. Ni, C.-W. Nan, L.-Z. Fan, InfoMat **4**, e12292 (2022)
67. B. Wang, G. Wang, P. He, L.-Z. Fan, J. Membr. Sci. **642**, 119952 (2022)
68. S. Randau, D.A. Weber, O. Kötz, R. Koerver, P. Braun, A. Weber, E. Ivers-Tiffée, T. Adermann, J. Kulisch, W.G. Zeier, F.H. Richter, J. Janek, Nat. Energy **5**, 259 (2020)
69. P. Angelopoulou, G. Avgouropoulos, Mater. Res. Bull. **119**, 110562 (2019)
70. T. Shi, Q. Tu, Y. Tian, Y. Xiao, L.J. Miara, O. Kononova, G. Ceder, Adv. Energy Mater. **10**, 1902881 (2020)
71. G.B. Appetecchi, M. Carewska, F. Alessandrini, P.P. Prosini, S. Passerini, J. Electrochem. Soc. **147**, 451 (2000)
72. B. Zhang, L. Chen, J. Hu, Y. Liu, Y. Liu, Q. Feng, G. Zhu, L.-Z. Fan, J. Power Sources **442**, 227230 (2019)
73. L. Zhao, Y. Zeng, L. Fu, J. Zhang, D. Sun, Y. Tang, Y. Ren, F. Pan, H. Wang, Small Struct. **3**, 2200200 (2022)
74. Y. Li, D. Zhang, X. Xu, Z. Wang, Z. Liu, J. Shen, J. Liu, M. Zhu, J. Energy Chem. **60**, 32 (2021)
75. J. Zong, X. Liu, Electrochim. Acta **116**, 9 (2014)
76. M. Sun, H. Li, J. Wang, G. Wang, Carbon **94**, 864 (2015)
77. S.W. Park, G. Oh, J.-W. Park, Y.-C. Ha, S.-M. Lee, S.Y. Yoon, B.G. Kim, Small **15**, 1900235 (2019)
78. S. Deng, Y. Sun, X. Li, Z. Ren, J. Liang, K. Doyle-Davis, J. Liang, W. Li, M. Norouzi Banis, Q. Sun, R. Li, Y. Hu, H. Huang, L. Zhang, S. Lu, J. Luo, X. Sun, ACS Energy Lett. **5**, 1243 (2020)
79. P. Ding, Z. Lin, X. Guo, L. Wu, Y. Wang, H. Guo, L. Li, H. Yu, Mater. Today **51**, 449 (2021)
80. Y. Kato, S. Shiotani, K. Morita, K. Suzuki, M. Hirayama, R. Kanno, J. Phys. Chem. Lett. **9**, 607 (2018)
81. K. Nie, Y. Hong, J. Qiu, Q. Li, X. Yu, H. Li, L. Chen, Front. Chem. **6**, 616 (2018)
82. Z. Li, H. Zhang, X. Sun, Y. Yang, ACS Energy Lett. **5**, 3244 (2020)
83. Y. Maeyoshi, D. Ding, M. Kubota, H. Ueda, K. Abe, K. Kanamura, H. Abe, ACS Appl. Mater. Interfaces **11**, 25833 (2019)
84. Y. Lin, X. Zhang, Y. Liu, Q. Wang, C. Lin, S. Chen, Y. Zhang, J. Colloid Interface Sci. **628**, 14 (2022)
85. X. Cao, X. Ren, L. Zou, M.H. Engelhard, W. Huang, H. Wang, B.E. Matthews, H. Lee, C. Niu, B.W. Arey, Y. Cui, C. Wang, J. Xiao, J. Liu, W. Xu, J.-G. Zhang, Nat. Energy **4**, 796 (2019)
86. X. Fan, L. Chen, X. Ji, T. Deng, S. Hou, J. Chen, J. Zheng, F. Wang, J. Jiang, K. Xu, C. Wang, Chem **4**, 174 (2018)
87. K. Yoshida, M. Nakamura, Y. Kazue, N. Tachikawa, S. Tsuzuki, S. Seki, K. Dokko, M. Watanabe, J. Am. Chem. Soc. **133**, 13121 (2011)
88. Z. Zeng, V. Murugesan, K.S. Han, X. Jiang, Y. Cao, L. Xiao, X. Ai, H. Yang, J.-G. Zhang, M.L. Sushko, J. Liu, Nat. Energy **3**, 674 (2018)
89. Y. Sun, F. Jin, J. Li, B. Liu, X. Chen, H. Dong, Y. Mao, W. Gu, J. Xu, Y. Shen, X. Wu, L. Chen, ACS Appl. Energy Mater. **3**, 12127 (2020)
90. Y. Kuai, F. Wang, J. Yang, H. Lu, Z. Xu, X. Xu, Y. NuLi, J. Wang, Mater. Chem. Front. **5**, 6502 (2021)
91. Y. Wang, J. Ju, S. Dong, Y. Yan, F. Jiang, L. Cui, Q. Wang, X. Han, G. Cui, Adv. Funct. Mater. **31**, 2101523 (2021)
92. Q. Ma, X.-X. Zeng, J. Yue, Y.-X. Yin, T.-T. Zuo, J.-Y. Liang, Q. Deng, X.-W. Wu, Y.-G. Guo, Adv. Energy Mater. **9**, 1803854 (2019)
93. W. Zha, Y. Xu, F. Chen, Q. Shen, L. Zhang, Solid State Ion. **330**, 54 (2019)
94. B. Tong, P. Wang, Q. Ma, H. Wan, H. Zhang, X. Huang, M. Armand, W. Feng, J. Nie, Z. Zhou, Solid State Ion. **358**, 115519 (2020)
95. C. Xue, X. Zhang, S. Wang, L. Li, C.-W. Nan, ACS Appl. Mater. Interfaces **12**, 24837 (2020)
96. J. Hu, C. Lai, K. Chen, Q. Wu, Y. Gu, C. Wu, C. Li, Nat. Commun. **13**, 7914 (2022)
97. V. Wurster, C. Engel, H. Graebe, T. Ferber, W. Jaegermann, R. Hausbrand, J. Electrochem. Soc. **166**, A5410 (2019)
98. R. Jung, M. Metzger, F. Maglia, C. Stinner, H.A. Gasteiger, J. Electrochem. Soc. **164**, A1361 (2017)
99. J. Qiu, X. Liu, R. Chen, Q. Li, Y. Wang, P. Chen, L. Gan, S.J. Lee, D. Nordlund, Y. Liu, X. Yu, X. Bai, H. Li, L. Chen, Adv. Funct. Mater. **30**, 1909392 (2020)
100. X. Lin, J. Yu, M.B. Effat, G. Zhou, M.J. Robson, S.C.T. Kwok, H. Li, S. Zhan, Y. Shang, F. Ciucci, Adv. Funct. Mater. **31**, 2109322 (2021)
101. Z. Lin, X. Guo, R. Zhang, M. Tang, P. Ding, Z. Zhang, L. Wu, Y. Wang, S. Zhao, Q. Zhang, H. Yu, Nano Energy **98**, 107330 (2022)
102. H. Miyashiro, Y. Kobayashi, S. Seki, Y. Mita, A. Usami, M. Nakayama, M. Wakihara, Chem. Mater. **17**, 5603 (2005)
103. M. Zhang, K. Zhou, D. Ma, H. Wang, X. Tang, M. Bai, F. Liu, Z. Wang, Y. Ma, Mater. Today **56**, 53 (2022)
104. W. Zhou, Z. Wang, Y. Pu, Y. Li, S. Xin, X. Li, J. Chen, J.B. Goodenough, Adv. Mater. **31**, 1805575 (2019)
105. J.B. Goodenough, Energy Environ. Sci. **7**, 14 (2014)
106. L. Chen, S. Venkatram, C. Kim, R. Batra, A. Chandrasekaran, R. Ramprasad, Chem. Mater. **31**, 4598 (2019)
107. J. Xu, R.D. Deshpande, J. Pan, Y.-T. Cheng, V.S. Battaglia, J. Electrochem. Soc. **162**, A2026 (2015)
108. E.K.W. Andersson, C. Sångeland, E. Berggren, F.O.L. Johansson, D. Kühn, A. Lindblad, J. Mindemark, M. Hahlin, J. Mater. Chem. A **9**, 22462 (2021)
109. Z. Hei, S. Wu, H. Zheng, H. Liu, H. Duan, Solid State Ion. **375**, 115837 (2022)
110. Y. Zhu, X. He, Y. Mo, ACS Appl. Mater. Interfaces **7**, 23685 (2015)
111. J. Ring, L. Laa, A. Limbeck, V. Vonk, S. Volkov, A. Nenning, J. Fleig, J. Electrochem. Soc. **170**, 060509 (2023)
112. S. Li, Y.-M. Chen, W. Liang, Y. Shao, K. Liu, Z. Nikolov, Y. Zhu, Joule **2**, 1838 (2018)
113. P.-J. Alarco, Y. Abu-Lebdeh, A. Abouimrane, M. Armand, Nat. Mater. **3**, 476 (2004)
114. D. Zhou, Y.B. He, R. Liu, M. Liu, H. Du, B. Li, Q. Cai, Q.H. Yang, F. Kang, Adv. Energy Mater. **5**, 1500353 (2015)
115. H. Maleki Kheimeh Sari, X. Li, Adv. Energy Mater. **9**, 1970151 (2019)
116. X. Ban, W. Zhang, N. Chen, C. Sun, J. Phys. Chem. C **122**, 9852 (2018)
117. X. Feng, D. Ren, X. He, M. Ouyang, Joule **4**, 743 (2020)
118. Z. Zhou, M. Li, X. Zhou, X. Ju, L. Yang, Appl. Energy **349**, 121690 (2023)
119. G. Abels, I. Bardenhagen, J. Schwenzel, F. Langer, J. Electrochem. Soc. **169**, 020560 (2022)
120. M.A. Webb, Y. Jung, D.M. Pesko, B.M. Savoie, U. Yamamoto, G.W. Coates, N.P. Balsara, Z.-G. Wang, T.F. Miller III, ACS Cent. Sci. **1**, 198 (2015)
121. H. Yang, N. Wu, Energy Sci. Eng. **10**, 1643 (2022)
122. Z. Zhang, S. Chen, X. Yao, P. Cui, J. Duan, W. Luo, Y. Huang, X. Xu, Energy Storage Mater. **24**, 714 (2020)

123. F. Zhang, Z. Wang, L. Wang, W. Li, A. Pan, H. Song, J. Xu, J. Hu, X. Wu, Chem. Eng. J. **435**, 135101 (2022)
124. J.C. Li, R.Q. Zhang, C.L. Wang, N.B. Wong, Phys. Rev. B **75**, 155408 (2007)
125. Z. Li, J. Fu, X. Zhou, S. Gui, L. Wei, H. Yang, H. Li, X. Guo, Adv. Sci. **10**, 2201718 (2023)
126. C.Y. Son, Z.-G. Wang, J. Chem. Phys. **153**, 100903 (2020)
127. K.D. Fong, J. Self, B.D. McCloskey, K.A. Persson, Macromolecules **54**, 2575 (2021)
128. V. Wurster, C. Engel, H. Gräbe, T. Ferber, W. Jaegermann, R. Hausbrand, J. Electrochem. Soc. **166**, A5410 (2019)
129. J. Mindemark, M.J. Lacey, T. Bowden, D. Brandell, Prog. Polym. Sci. **81**, 114 (2018)
130. S.B. Aziz, Appl. Phys. A **122**, 706 (2016)
131. N. Kaiser, S. Spannenberger, M. Schmitt, M. Cronau, Y. Kato, B. Roling, J. Power Sources **396**, 175 (2018)
132. Y. Zhong, C. Cao, M.O. Tadé, Z. Shao, ACS Appl. Mater. Interfaces **14**, 38786 (2022)
133. J. Landesfeind, J. Hattendorff, A. Ehrl, W.A. Wall, H.A. Gasteiger, J. Electrochem. Soc. **163**, A1373 (2016)
134. J. Landesfeind, M. Ebner, A. Eldiven, V. Wood, H.A. Gasteiger, J. Electrochem. Soc. **165**, A469 (2018)
135. B.L. Trembacki, A.N. Mistry, D.R. Noble, M.E. Ferraro, P.P. Mukherjee, S.A. Roberts, J. Electrochem. Soc. **165**, E725 (2018)
136. L. Almar, J. Joos, A. Weber, E. Ivers-Tiffée, J. Power Sources **427**, 1 (2019)
137. J. Evans, C.A. Vincent, P.G. Bruce, Polymer **28**, 2324 (1987)
138. Z. Zeng, J. Cheng, Y. Li, H. Zhang, D. Li, H. Liu, F. Ji, Q. Sun, L. Ci, Mater. Today Phys. **32**, 101009 (2023)
139. H. Yuan, H.-X. Nan, C.-Z. Zhao, G.-L. Zhu, Y. Lu, X.-B. Cheng, Q.-B. Liu, C.-X. He, J.-Q. Huang, Q. Zhang, Batteries & Supercaps **3**, 596 (2020)
140. Y. Lu, C.-Z. Zhao, H. Yuan, J.-K. Hu, J.-Q. Huang, Q. Zhang, Matter **5**, 876 (2022)
141. X. Yang, Q. Sun, C. Zhao, X. Gao, K.R. Adair, Y. Liu, J. Luo, X. Lin, J. Liang, H. Huang, L. Zhang, R. Yang, S. Lu, R. Li, X. Sun, Nano Energy **61**, 567 (2019)
142. L. Helmers, L. Froböse, K. Friedrich, M. Steffens, D. Kern, P. Michalowski, A. Kwade, Energy Technol. **9**, 2000923 (2021)
143. C. Huang, C.L.A. Leung, P. Leung, P.S. Grant, Adv. Energy Mater. **11**, 2002387 (2021)
144. S.Z. Zhang, X.H. Xia, D. Xie, R.C. Xu, Y.J. Xu, Y. Xia, J.B. Wu, Z.J. Yao, X.L. Wang, J.P. Tu, J. Power Sources **409**, 31 (2019)